Neurobiology of Aging 89 (2020) 118–128

Contents lists available at ScienceDirect

Neurobiology of Aging

journal homepage: www.elsevier.com/locate/neuaging

Diffusion MRI biomarkers of white matter microstructure vary nonmonotonically with increasing cerebral amyloid deposition

Jian W. Dong [a,b,1], Ileana O. Jelescu [a,c,1], Benjamin Ades-Aron [a], Dmitry S. Novikov [a], Kent Friedman [a], James S. Babb [a], Ricardo S. Osorio [d,e], James E. Galvin [f], Timothy M. Shepherd [a], Els Fieremans [a,*]

[a] Department of Radiology, New York University School of Medicine, New York, NY, USA
[b] Department of Radiology, Brigham & Women's Hospital, Harvard Medical School, Boston, MA, USA
[c] Centre d'Imagerie Biomédicale, École Polytechnique Fédérale de Lausanne, Lausanne, Switzerland
[d] Center for Sleep and Brain Health, Department of Psychiatry, NYU Langone Medical Center, New York, NY, USA
[e] Nathan S. Kline Institute for Psychiatric Research, Orangeburg, NY, USA
[f] Comprehensive Center for Brain Health, Department of Neurology, University of Miami Miller School of Medicine, Boca-Raton, FL, USA

ARTICLE INFO

Article history:
Received 23 November 2018
Received in revised form 14 December 2019
Accepted 14 January 2020
Available online 23 January 2020

Keywords:
Diffusion MRI
Kurtosis
White matter
White matter tract integrity
Amyloid
Alzheimer

ABSTRACT

Beta amyloid (Aβ) accumulation is the earliest pathological marker of Alzheimer's disease (AD), but early AD pathology also affects white matter (WM) integrity. We performed a cross-sectional study including 44 subjects (23 healthy controls and 21 mild cognitive impairment or early AD patients) who underwent simultaneous PET-MR using 18F-Florbetapir, and were categorized into 3 groups based on Aβ burden: Aβ− [mean mSUVr ≤1.00], Aβi [1.00 < mSUVr <1.17], Aβ+ [mSUVr ≥1.17]. Intergroup comparisons of diffusion MRI metrics revealed significant differences across multiple WM tracts. Aβi group displayed more restricted diffusion (higher fractional anisotropy, radial kurtosis, axonal water fraction, and lower radial diffusivity) than both Aβ− and Aβ+ groups. This nonmonotonic trend was confirmed by significant continuous correlations between mSUVr and diffusion metrics going in opposite direction for 2 cohorts: pooled Aβ−/Aβi and pooled Aβi/Aβ+. The transient period of increased diffusion restriction may be due to inflammation that accompanies rising Aβ burden. In the later stages of Aβ accumulation, neurodegeneration is the predominant factor affecting diffusion.

1. Introduction

Alzheimer's disease (AD) is neuropathologically defined by the accumulation of beta amyloid (Aβ) plaques and tau protein hyperphosphorylation in gray matter structures particularly the cerebral cortex and hippocampus. Although classic macroscopic structural changes such as hippocampal atrophy and parenchymal volume loss can be detected in the later stages of mild cognitive impairment (MCI) and AD using conventional magnetic resonance imaging (MRI), the pathogenesis of AD long precedes its clinical symptoms, often by decades (Jack et al., 2013), making preclinical diagnosis difficult. One of the earliest pathological findings in AD is the accumulation of Aβ plaques in the cerebral cortex, which can be detected in vivo with Aβ PET imaging radiotracers such as florbetapir before the onset of clinical manifestations (Clark et al., 2011; Sperling et al., 2011; Wong et al., 2010) with high sensitivity (88%–98%) and specificity (88%–100%) (Clark et al., 2012; Curtis et al., 2015; Sabri et al., 2015). Aβ plaques are a necessary but insufficient marker for clinical deterioration, consistent with recent evidence of synergistic effects between Aβ burden and hippocampal atrophy (Bilgel et al., 2018), and with the research framework of AD considering the presence of amyloid, tau, and neurodegeneration to stage cases along a pathobiological continuum (Jack et al., 2018).

Although the pathogenesis of AD was historically considered a disease of gray matter, white matter (WM) damage has been observed histologically in *postmortem* patients with early AD as partial loss of myelin, axons, and oligodendroglial cells, as well as the presence of reactive astrocytic gliosis (Brun and Englund, 1986; Englund et al., 1988; Gottfries et al., 1996; Kemper, 1994; Kobayashi et al., 2002; Malone and Szoke, 1985; Roher et al., 2002; Svennerholm and Gottfries, 1994). WM structure can be monitored in vivo using diffusion MRI. The most widely used diffusion

* Corresponding author at: Department of Radiology, New York University School of Medicine, 660 First Avenue, room 205, New York, NY 10016, USA. Tel./fax: +1 212 263 3344.
E-mail address: Els.Fieremans@nyulangone.org (E. Fieremans).
[1] These authors contributed equally to the work.

0197-4580/$ – see front matter © 2020 Elsevier Inc. All rights reserved.
https://doi.org/10.1016/j.neurobiolaging.2020.01.009

MRI method is diffusion tensor imaging (DTI) (Basser and Pierpaoli, 1996), which quantifies the Gaussian part of the diffusion displacement distribution, characterized by the diffusion tensor and its derived metrics including the mean, axial and radial diffusivity (RD), and fractional anisotropy (FA). The FA is a marker of orientation coherence for diffusion, whereas the RD is the diffusivity transverse to the main fiber orientation, with both being used as empirical markers of WM integrity. Multiple studies have consistently shown that subjects with MCI and early AD exhibit WM alterations indicative of reduced integrity/complexity with reduced FA, and increased mean, axial, and radial diffusivities in normal-appearing WM tracts of the temporal, parietal, and frontal lobes compared to healthy elderly control subjects (Agosta et al., 2011; Madden et al., 2009; Mayo et al., 2017; Wurtman, 2015). Several DTI studies also have highlighted a strong correlation between WM alterations and cognitive performance (Chang et al., 2015; Di Paola et al., 2015; Kantarci et al., 2014; Mielke et al., 2009), as well as high prediction value for future memory decline (Mielke et al., 2012).

Despite these findings of reduced WM integrity in AD, the exact underlying pathologic changes of these diffusion markers and their timeline in the clinical course of AD are undefined, and the temporal relation of WM changes with respect to amyloid deposition is not well characterized. In particular, there are conflicting studies of WM changes as measured with DTI with respect to amyloid burden, reporting either increased diffusion restriction [reflected by a respectively lower mean diffusivity (MD) and higher FA (Racine et al., 2014)] or reduced diffusion restriction [reflected by a higher MD (Chao et al., 2013; Pietroboni et al., 2017) or lower FA (Chao et al., 2013)] in WM with increasing amyloid load. A decoupling between amyloid status and WM degeneration also has been reported (Kantarci et al., 2014; Mito et al., 2018).

In this study, we use diffusion kurtosis imaging (DKI), a clinically feasible extension of DTI that accounts also for non-Gaussian diffusion properties of nervous tissue and thus provides additional information on tissue complexity (Jensen and Helpern, 2010). DKI includes standard DTI metrics such as FA and RD, as well as additional kurtosis metrics such as radial kurtosis (RK). DKI also allows for estimating the white matter tract integrity (Fieremans et al., 2011) model including quantification of the axonal water fraction (AWF), which is the relative (T_2-weighted) signal fraction from water inside the axons (and potentially glial processes) over the total water fraction (from water both inside and outside axons, excluding myelin water due to its short T_2). Using the cuprizone-fed mouse model (Guglielmetti et al., 2016; Jelescu et al., 2016b), the diffusion MRI–derived AWF has been recently validated against AWF derived from electron microscopy images and has been shown to be sensitive to both patchy demyelination and axonal degeneration taking place during the acute (6 weeks) and chronic (12 weeks) phases of cuprizone intoxication, respectively.

As applied to the study of aging and AD, both DKI metrics and AWF have been shown previously to differentiate AD from MCI (Fieremans et al., 2013) and to be altered first in vulnerable late-myelinating WM tracts compared to early myelinating tracts (Benitez et al., 2013, 2018). This is indicative of demyelination and potential axonal degeneration in these bundles during the AD pathologic cascade.

The goals of the present study are to use DKI metrics and AWF to identify WM tracts affected by AD pathology and to characterize the relationship between WM microstructural changes and Aβ deposition in both cognitively healthy and cognitively impaired populations. This way, we aim to better understand the mechanisms that may be involved in the pathogenesis of AD, and in its prodromal stage, MCI.

2. Methods

2.1. Subjects

This study was approved by the local Institutional Review Board. Fifty-two subjects were recruited from an Alzheimer Disease Center in a cross-sectional study design of cognitively normal or early cognitively impaired patients. Per protocol, all subjects received neurological and neuropsychological evaluations in addition to integrated PET/MR imaging. PET and MR were separately reviewed by a nuclear medicine physician and a board-certified neuroradiologist, respectively, before inclusion in this study. Of the 52 subjects initially recruited, 8 subjects in total were excluded due to motion degradation ($n = 1$), comorbidities (traumatic brain injury or severe depression, $n = 2$), or alternative explanations for cognitive impairment (primary progressive aphasia, posterior cortical atrophy, severe ischemic WM disease, frontotemporal dementia, or cerebellar ataxia, $n = 5$) as suggested by medical history and/or imaging examination. Ultimately, 44 subjects (mean age 69.0 ± 5.1 years, range 56–79 years; 24 females) were included in this study.

All participants were comprehensively evaluated by board-certified neurologists, psychiatrists, and neuropsychologists using the Uniform Data Set from the National Institute on Aging Alzheimer Disease Center Program (Morris et al., 2006; Weintraub et al., 2009). Clinical diagnosis was derived at consensus conference using standard criteria for AD (McKhann et al., 2011) and MCI thought to be due to underlying AD (Albert et al., 2011; Petersen et al., 2001). Global cognitive status was staged using the Global Deterioration Scale (GDS) (Reisberg et al., 1982). A GDS score of 1 corresponds to normal cognition, GDS score of 2 corresponds to subjective cognitive impairment, GDS score of 3 corresponds to MCI, and GDS score of 4 represents mild dementia. Although developed in 1982, the GDS staging closely aligns with the research clinical stages of the AD continuum proposed by Jack and colleagues (Jack et al., 2018). In our analyses, GDS scores of 1 and 2 combine to represent normal controls, GDS score of 3 represents MCI, and GDS score of 4 represents mild AD.

2.2. Acquisition

Subjects were scanned on a 3-T integrated PET-MRI system (Siemens Biograph mMR, VB20) after obtaining informed consent. A dose of 9 mCi of 18F-Florbetapir (Eli Lilly) was injected intravenously and PET list-mode data were acquired for 20 minutes starting at 40 minutes after injection. One static uptake image was reconstructed (Wong et al., 2010) using the Siemens e7tools combined with a VB20 Siemens Ultrashort Echo Time–based attenuation map ($TE_1 = 0.07$ ms, $TE_2 = 2.46$ ms, resolution = 1.6 mm isotropic). This attenuation correction was performed to account for standardized uptake value (SUV) inaccuracy in air, bone, and soft tissue and has been shown to exhibit robust reduction of attenuation-related artifacts (Aasheim et al., 2015). PET reconstruction parameters were—algorithm: OP-OSEM (ordinary Poisson ordered subset expectation maximization) with 3 iterations and 21 subsets; matrix: 344 × 344; 2 mm-kernel Gaussian filter; zoom 2.

MRI data were acquired using a 12-channel phased array RF coil. An anatomical MP-RAGE was acquired (TE = 2.98 ms, TR = 2.3s, TI = 900 ms, flip angle = 9°, resolution = 1 mm isotropic) for cortical segmentation. A FLAIR image (FLuid Attenuated Inversion Recovery) was acquired to evaluate WM lesion load (32 axial slices, slice thickness = 5 mm, in-plane resolution = 750 × 692 μm^2, TE = 91 ms, TR = 8 second, inversion time = 2.37s, flip angle = 150°). For the derivation of diffusion tensor, kurtosis tensor, and AWF (Fieremans et al., 2011), a total of 140 diffusion-weighted images were acquired as follows: 4 $b = 0$ images, $b = 250$ s/mm^2–6 directions,

$b = 1000$ s/mm^2–20 directions, $b = 1500$ s/mm^2–20 directions, $b = 2000$ s/mm^2–30 directions, $b = 2500$ s/mm^2–60 directions. Twice refocused spin-echo single-shot echo-planar imaging was performed with TE = 96 ms, TR = 8.2 second, 50 slices, resolution = 2.5 mm isotropic, GRAPPA acceleration factor of 2. To correct for echo-planar imaging distortions secondary to magnetic field inhomogeneity [combined with eddy current correction in FSL's EDDY tool (Andersson and Sotiropoulos, 2016)], 6 additional b = 0 images were acquired with reverse phase-encode direction (posterior-anterior instead of anterior-posterior).

2.3. Image processing

2.3.1. Structural volume

Automatic cortical and subcortical segmentation was performed on the MP-RAGE sequence using FreeSurfer v5.3.0 (http://surfer.nmr.mgh.harvard.edu/). For each subject, the volume of the following gray matter regions of interest (ROIs) was extracted: hippocampus, medial temporal lobe structures (comprised the entorhinal cortex, fusiform, and parahippocampal gyri), parietal lobe (comprised the inferior parietal, superior parietal, and precuneus), anterior cingulate cortex, posterior cingulate cortex, and medio-orbital frontal lobe. Each region volume was normalized to the estimated total intracranial volume of each subject.

2.3.2. WM lesions

WM lesions were automatically segmented on the FLAIR images using FireVoxel (Mikheev et al., 2008) and accuracy of segmentation was reviewed by a board-certified neuroradiologist. The total WM lesion volume was subsequently calculated and normalized to the total intracranial volume (Bilello et al., 2015) computed using the FreeSurfer anatomical segmentation for each subject.

2.3.3. Florbetapir uptake

The reconstructed PET image was registered to the MR anatomical image using FSL's linear registration function "FLIRT" (Jenkinson et al., 2002) with a mutual information cost function. Using the structural masks obtained from FreeSurfer (see above section 2.3.1), the mean SUV was calculated in 5 cortical ROI known for pathological uptake of florbetapir (anterior cingulate, posterior cingulate, medial orbito-frontal lobe, parietal lobe, and medial temporal lobe), normalized to the mean SUV in the cerebellum to yield relative SUV (SUVr) (Clark et al., 2011). Averaging across all 5 regions yielded the mean SUVr (mSUVr) for each subject. Each region was given the same weight upon averaging (i.e., not accounting for region size), per initial definition of the mSUVr (Clark et al., 2012). SUVr values below 1 are possible given nonpathological uptake of florbetapir in cerebellar WM (Joshi et al., 2012).

2.3.4. Subject classification

Using a lower mSUVr threshold of 1.00 and upper mSUVr threshold of 1.17, subjects were categorized into Aβ low, Aβ intermediate, or Aβ high (denoted as Aβ−, Aβi, or Aβ+, respectively). An mSUVr less than or equal to 1.00 denoted that the amyloid load in the cerebral cortex was equal or less than that the reference region. An mSUVr equal to or greater than 1.17 has been shown to be an accurate threshold used to reflect pathological levels of amyloid based on postmortem neuropathology data (Fleisher et al., 2011). Values of mSUVr between 1.00 and 1.17 were considered equivocal for pathological level of amyloid.

2.3.5. Diffusion metrics

Processing and tensor estimation were performed using the DESIGNER pipeline (Ades-Aron et al., 2018) (https://github.com/NYU-DiffusionMRI/DESIGNER) and included "Marchenko-Pastur Principal Component Analysis" denoising (Veraart et al., 2016a,b), Gibbs artifacts correction (Kellner et al., 2016), Rician bias correction, eddy current and motion correction (Andersson and Sotiropoulos, 2016), followed by CSF-excluded smoothing using a Gaussian filter with full-width-half-maximum of 2.5 mm. The kurtosis tensor was estimated in each voxel using a weighted linear least squares fit (Veraart et al., 2013) in MATLAB (The MathWorks, Natick, MA). Parametric maps of FA, RD, and RK were derived from the diffusion and kurtosis tensors. We focused on the radial metrics given their sensitivity to myelin and axonal changes in the white matter (Jelescu et al., 2016b). In addition, the white matter tract integrity (WMTI) parameter estimation framework was used to derive AWF based on the kurtosis tensor (Fieremans et al., 2011). AWF estimated from WMTI was shown to correlate with tissue axonal volume fraction from histology (Jelescu et al., 2016b). Its accuracy relies on the fact that it does not rely on the "branch choice" assumptions based on the compartment diffusivity values (Fieremans et al., 2011), that are an active topic of investigation (Jelescu et al., 2015, 2016a; Kunz et al., 2018; Novikov et al., 2018, 2019). Parametric maps from a representative subject from each group are provided as Supplementary Figs. 1-3.

2.3.6. Voxel-wise analysis

Using FSL's tract-based spatial statistics (TBSS), standardized skeletonized voxel-wise analyses were performed to identify areas where significant differences in diffusion metrics (Smith et al., 2006) occurred between groups. Briefly, the Johns Hopkins University (JHU) White Matter FA template (Mori et al., 2008) was used as a target for registration of each subject's FA map using FSL's nonlinear registration tool (Andersson et al., 2007; Jenkinson et al., 2012), from which the mean FA map was computed and projected onto a WM skeleton, representing the center of WM tracts. A threshold of FA > 0.4 was chosen to ensure that the skeleton represented areas of high fiber unidirectionality, which is a regime where the WMTI model is applicable and where the AWF estimation has been shown to agree with that from more advanced models that can account for fiber dispersion, such as Fiber Ball Imaging (McKinnon et al., 2018). Finally, each diffusion metric parametric map (FA, RD, RK, AWF) was projected onto the thresholded WM skeleton before statistical analysis.

2.3.7. Region of interest analysis

For each subject, the FA map was registered to the JHU template (Mori et al., 2008) using the nonlinear transformation computed during TBSS analysis. All WM regions of interest (ROIs) were then warped from the JHU Atlas into native subject space. For each subject, mean and standard deviations for FA, RD, RK, and AWF were extracted in 9 WM ROIs that were chosen based on their (early) involvement in AD pathogenesis (Chao et al., 2013; Oishi and Lyketsos, 2014; Racine et al., 2014; Wolf et al., 2015): fornix, genu, and body of the corpus callosum (cc), anterior limb of the internal capsule (left and right), anterior corona radiata (left and right), and superior corona radiata (left and right). Quantitative comparison of these 4 metrics among the 3 Aβ groups was performed for each WM ROI.

2.3.8. Statistical methods

For both voxel-wise and ROI-based approaches, we performed a one-way ANCOVA analysis between Aβ−, Aβi, and Aβ+ groups for each diffusion parameter of interest, with group membership acting as the independent variable and controlling for patient age and sex. Similar ANCOVA analyses were also performed controlling for age, sex, and GDS. For the voxel-wise approach, a nonparametric statistical analysis was performed using FSL's "randomize" (Winkler et al., 2014), with 5000 permutations along with threshold-free cluster enhancement (Smith and Nichols, 2009) to correct for

Table 1
Mean demographics and clinical characteristics for Aβ−, Aβi, and Aβ+ groups (N = 44)

Parameter	Aβ− (n = 13)	Aβi (n = 22)	Aβ+ (n = 9)	χ^2/F-test	*p* value
Age	67.7 ± 5.8	69.5 ± 5.0	69.8 ± 4.7	N/A	0.616
No. of females	5/13 (38%)	15/22 (68%)	4/9 (44%)	3.4	0.185
No. of cognitive normal	10/13 (77%)	11/22 (50%)	2/9 (22%)	12.6	0.013
No. of MCI	3/13 (23%)	11/22 (50%)	5/9 (56%)		
No. of AD	0/13 (0%)	0/22 (0%)	2/9 (22%)		

Subjects are age- and sex-matched across groups. Mental status is significantly different across groups ($p = 0.013$). ANOVA test for age, chi-square test for sex, chi-square test for cognitive status (healthy control vs. MCI vs. AD).
Key: AD, Alzheimer's disease; MCI, mild cognitive impairment.

multiple comparisons between groups, and obtain group differences between voxels at a significance level of $p < 0.05$. Significant differences in voxel-based clusters were projected onto the WM skeleton to visualize statistical comparison results. For the ROI approach, the threshold for statistically significant group differences was $p < 0.05$ after applying Tukey's Honest Significant Difference criterion (Tukey's HSD) for comparing 3 independent groups. To further confirm our findings, we additionally performed partial Pearson correlations (covarying for age, sex, and GDS) relative to mSUVr in 2 groups, created by combining the Aβ−/Aβi groups into a single cohort, and Aβi/Aβ+ groups into a single cohort.

3. Results

3.1. Participant characteristics

The subject demographics categorized by Aβ level are listed in Table 1. Of the 44 subjects, 13 (30%) were classified as Aβ−, 22 (50%) as Aβi, and 9 (20%) as Aβ+. There were no significant differences among Aβ groups in terms of age ($p = 0.61$, ANOVA) or sex ($\chi^2 = 3.4$, $p = 0.18$, χ^2 test). Statistical difference was observed among the Aβ groups based on cognitive status ($\chi^2 = 12.6$, $p = 0.01$, χ^2 test). Among the Aβ- cohort, 10/13 (77%) were cognitively normal, and 3/13 had MCI. Among the Aβi cohort, 11/22 (50%) were cognitively normal and 11/22 had MCI. Among the Aβ+ cohort, 2/9 (22%) were cognitively normal, 5/9 (56%) had mild cognitive impairment, and 2/9 had clinical AD.

The mean hippocampal volume [% of total intracranial volume] was 0.49, 0.54, and 0.40, respectively, for Aβ−, Aβi, Aβ+ groups ($p = 0.06$ for Aβ−/Aβi comparison, $p = 0.05$ for Aβ−/Aβ+ comparison, and $p < 0.01$ for Aβi/Aβ+ comparison, ANCOVA covarying for age and corrected for multiple comparisons using Tukey's HSD). There was no difference in WM lesion load among the 3 groups ($p = 0.80$ for Aβ−/Aβi comparison, $p = 0.56$ for Aβ−/Aβ+ comparison, $p = 0.84$ for Aβi/Aβ+ comparison, ANCOVA covarying for age and corrected for multiple comparison using Tukey's HSD). These neuroimaging characteristics are summarized in Table 2. A plot of mSUVr versus age is shown in Fig. 1.

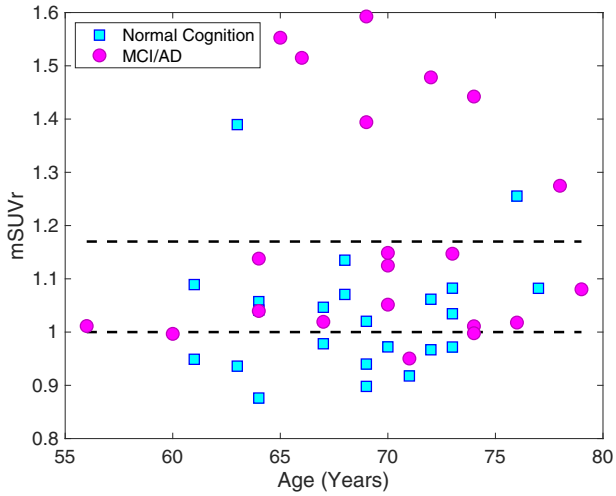

Fig. 1. Plot of mSUVr versus age, categorized by cognitive status. Subjects with lower amyloid burden correlate with lower prevalence of impaired cognitive status (77% of Aβ− subjects are cognitively normal, compared to 50% in Aβi, and 22% in Aβ+, $p = 0.013$, chi-square test). Aβ−: mSUVr ≤1.1, Aβi: 1.1 < mSUVr <1.17, Aβ+: mSUVr ≥1.17.

TBSS voxel-wise analyses are summarized in Fig. 2. TBSS detected differences in FA, RD, RK, AWF between Aβ− versus Aβi, and in FA, RK, AWF between Aβi and Aβ+ groups. Most notably, group differences were found in the genu of the corpus callosum between Aβ−/Aβi for all diffusion parameters and between Aβi/Aβ+ for RK, and AWF ($p < 0.01$). From Aβ− to Aβi, there was an overall increase in diffusion restriction as shown by decreasing RD, and increasing FA, RK, and AWF. Interestingly, from Aβi to Aβ+, the diffusion differences implied an overall decrease in diffusion restriction, as shown by lower FA, RK, and AWF.

While these opposing changes were predominantly observed in the genu of the corpus callosum and anterior corona radiata, we also found similar differences in the fornix. The latter however disappeared after cluster-wise correction for multiple comparisons, possibly because of the small size of this region and increased partial volume effects with CSF due to AD-related fornix atrophy (Oishi and Lyketsos, 2014). The uncorrected TBSS results are shown as Supplementary Fig. 4.

3.2. ROI analysis: group comparisons

The nonmonotonic diffusion metric changes between Aβ−/Aβi and Aβi/Aβ+ as observed in the TBSS analysis also were observed in independent ROI analyses of the WM tracts defined based on the JHU WM Atlas, summarized in Table 3. The most notable significant changes were found in the fornix and the genu of the corpus callosum, but the nonmonotonic trend also appeared diffusely, including the body of corpus callosum and anterior corona radiata. Corresponding boxplots are shown in Fig. 3 for the fornix and Fig. 4 for the genu of the corpus callosum. Results were not altered by

Table 2
Neuroimaging characteristics of Aβ−, Aβi, and Aβ+ groups (N = 44)

Parameter	Aβ− (n = 13)	Aβi (n = 22)	Aβ+ (n = 9)	*p* value (Aβ−/Aβi)	*p* value (Aβ−/Aβ+)	*p* value (Aβi/Aβ+)
mSUVr	0.95 ± 0.04	1.07 ± 0.05	1.43 ± 0.11	<0.001	<0.001	<0.001
Standardized hippocampal volume [% of TIV]	0.49 ± 0.05	0.54 ± 0.08	0.40 ± 0.07	0.061	0.048	<0.001
WM lesion load [% of TIV]	0.14 ± 0.29	0.10 ± 0.19	0.07 ± 0.09	0.794	0.567	0.844

Standardized hippocampal volume differed significantly only in the Aβi/Aβ+ comparison. ANCOVA, covarying for age, corrected for multiple comparisons (e.g., Aβ−/Aβi, Aβ−/Aβ+, and Aβi/Aβ+ comparisons) using Tukey's HSD.
Key: TIV, total intracranial volume.

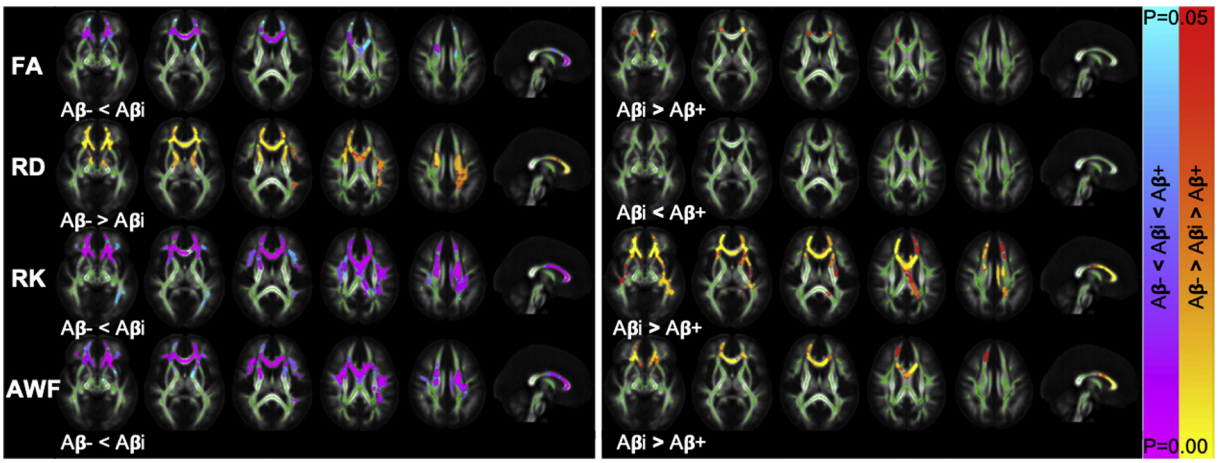

Fig. 2. TBSS results: Axial and midsagittal views show significant differences between Aβ−/Aβi groups and Aβi/Aβ+ groups for FA (row 1), RD (row 2), RK (row 3), and AWF (row 4). Clusters of increased (red/orange) and lower (blue/purple) are overlaid on the FA template, together with the mean skeleton (green). The observed differences between Aβ−/Aβi comparison are in the opposite direction of those in Aβi/Aβ+ comparison. TBSS revealed significant differences involving the genu of the corpus callosum and the anterior corona radiata. Directions of changes are consistent as those observed in the ROI analysis. Abbreviations: AWF, axonal water fraction; FA, fractional anisotropy; RD, radial diffusivity; ROI, region of interest; RK, radial kurtosis; TBSS, tract-based spatial statistics.

inclusion of GDS as a covariate (not shown), which suggests the relationship between amyloid burden and white matter integrity is not likely to be directly driven by underlying relationships between amyloid burden and cognitive status on the one hand, and cognitive status and white matter integrity on the other hand. In addition to FA, RD, RK, and AWF, we observed similar changes across diffusion metrics such as MD and kurtosis, as well as axial diffusivity and kurtosis, provided in Supplementary Table 1.

3.3. ROI analysis: correlation analysis of mSUVr versus diffusion metrics

To examine the overall trend between amyloid low and high groups, we additionally combined the Aβ−/Aβi groups into a single cohort, and Aβi/Aβ+ groups into a single cohort. Separately for each cohort, we analyzed the correlations between each diffusion metric (FA, RD, DK, AWF) and to mSUVr (with amyloid burden as a continuous variable) using age-, sex-, and GDS-controlled Pearson regression in 2 selected regions of interest known to be involved (fornix and genu of the corpus callosum) in AD pathology. With the exception of RD in the Aβ−/Aβi cohort in the genu of the corpus callosum, we found significant correlations between all diffusion metrics and mSUVr among both cohorts, and in both ROIs (Figs. 5 and 6). Furthermore, the sign of the correlation coefficient was opposite between the 2 cohorts, for example, AWF correlated positively with SUVr in the Aβ−/Aβi cohort and negatively in the Aβi/Aβ+ cohort. This further validates the observed nonmonotonic changes and highlights that the voxel-wise and ROI analyses presented previously do not depend strongly on the precise SUVr threshold chosen to separate Aβ−, Aβi, and Aβ+ groups.

4. Discussion

We reported diffusion metrics in cognitively normal and impaired subjects with varying Aβ levels using integrated PET/MR imaging. Subjects were grouped into low, intermediate, and high Aβ levels, based on binding of 18F-Florbetapir in selected cortical regions known for pathological uptake (Clark et al., 2011). Using 2 independent methods—TBSS and ROI analysis of WM tracts defined by the JHU WM Atlas—we measured the group means of diffusion metrics as a function of Aβ levels, and found changes in opposing directionality that were most notable in the genu of the corpus callosum and fornix, and further supported by correlational analyses in these regions. Findings also were more extensively spread in anterior cerebral WM tracts such as the anterior corona radiata. We found a pattern suggesting more diffusion restriction at intermediate amyloid burden (between Aβ− and Aβi groups)—as indicated by higher FA, RK, and AWF and lower RD—and less diffusion restriction at higher amyloid burden (between Aβi and Aβ+ groups)—as indicated by lower FA, RK, and AWF and higher RD. RK and AWF parameters showed the most robust and significant changes, supporting the value of studying advanced models of tissue water diffusion in addition to traditional DTI.

Previous DTI-based studies assessing the relationship between WM structure and cerebral amyloid load measured with PiB (Chao et al., 2013; Racine et al., 2014; Wolf et al., 2015) or CSF Aβ levels (Pietroboni et al., 2017) observed changes in parts of the cingulum, corona radiata, and corpus callosum. However, the reported directions of changes in DTI metrics are not well agreed upon. On the one hand, 2 studies spanning subjects who were cognitively normal or mild cognitively impaired found that Aβ positivity was associated with reduced FA in the fornix and splenium of the corpus callosum (Chao et al., 2013; Pietroboni et al., 2017), or an increased MD in WM lesions (Pietroboni et al., 2017). Yet another study found increased FA and lower MD with cerebral amyloid deposition in cognitively healthy subjects separated into Aβ−, Aβi, and Aβ+ groups defined based on specific PiB threshold uptake (Racine et al., 2014). This study's finding between Aβ− and Aβi is concordant with our results, but they did not report divergent changes observed in the present study between Aβi and Aβ+. A recent DTI study of ADNI data reported a nonlinear association between global WM diffusion metrics and PiB amyloid deposition (Wolf et al., 2015) which is also consistent with the present study. Our study expands on these previous studies by including higher order diffusion metrics (i.e., DKI parameters and AWF) in addition to DTI, and by identifying the specific WM tracts involved in early AD, among 3 categorizable levels of amyloid burden (low, intermediate, high) in cognitively healthy controls and MCI/AD. Although DKI metrics are sensitive but not specific to features of microstructure, the AWF derived from the WMTI model provides a specific measure of the relative size of the intra- versus the extra-axonal compartments, weighted by their respective T_2 values. Our findings were not altered when including

Table 3
Independent region of interest analysis demonstrated nonlinearity in diffusion metrics with respect to amyloid burden

ROI	Metric	Aβ- (AVG±STD)	Aβi (AVG±STD)	Aβ+ (AVG±STD)	Aβ−/Aβi	Aβ−/Aβ+	Aβi/Aβ+
Fornix	FA	0.32 ± 0.06	0.37 ± 0.06	0.26 ± 0.06	*0.036	0.117	*<0.001
	RD	2.05 ± 0.44	1.62 ± 0.44	2.6 ± 0.52	*0.008	0.086	*<0.001
	RK	0.76 ± 0.14	0.88 ± 0.16	0.58 ± 0.13	*0.018	*0.037	*<0.001
	AWF	0.21 ± 0.03	0.24 ± 0.04	0.17 ± 0.03	*0.018	0.053	*<0.001
Genu of CC	FA	0.49 ± 0.05	0.52 ± 0.04	0.48 ± 0.04	*0.004	0.986	*0.023
	RD	1.04 ± 0.16	0.96 ± 0.11	1.11 ± 0.13	*0.013	0.784	*0.007
	RK	1.28 ± 0.14	1.38 ± 0.13	1.21 ± 0.17	*0.002	0.860	*0.013
	AWF	0.32 ± 0.03	0.34 ± 0.03	0.31 ± 0.02	*0.002	0.958	*0.005
Body of CC	FA	0.59 ± 0.05	0.60 ± 0.05	0.56 ± 0.05	0.503	0.612	0.142
	RD	0.72 ± 0.11	0.68 ± 0.10	0.76 ± 0.11	0.268	0.808	0.148
	RK	1.68 ± 0.14	1.79 ± 0.17	1.58 ± 0.32	*0.027	0.833	0.179
	AWF	0.39 ± 0.03	0.40 ± 0.03	0.38 ± 0.04	0.070	0.974	0.210
Anterior limb of internal capsule (right)	FA	0.52 ± 0.03	0.54 ± 0.03	0.53 ± 0.02	0.211	0.362	0.952
	RD	0.64 ± 0.06	0.58 ± 0.05	0.57 ± 0.05	*0.025	*0.016	0.754
	RK	1.56 ± 0.09	1.60 ± 0.09	1.52 ± 0.19	0.304	0.948	0.561
	AWF	0.39 ± 0.02	0.40 ± 0.02	0.39 ± 0.03	0.225	0.994	0.476
Anterior limb of internal capsule (left)	FA	0.50 ± 0.04	0.52 ± 0.04	0.50 ± 0.03	0.148	0.982	0.263
	RD	0.63 ± 0.10	0.58 ± 0.07	0.60 ± 0.07	0.121	0.537	0.634
	RK	1.51 ± 0.12	1.55 ± 0.11	1.40 ± 0.13	0.261	0.316	*0.015
	AWF	0.38 ± 0.03	0.39 ± 0.02	0.37 ± 0.02	0.162	0.841	*0.040
Anterior corona radiata (right)	FA	0.37 ± 0.04	0.39 ± 0.03	0.38 ± 0.02	*0.029	0.415	0.455
	RD	0.81 ± 0.09	0.75 ± 0.05	0.80 ± 0.09	*0.009	0.608	0.178
	RK	1.16 ± 0.10	1.20 ± 0.08	1.10 ± 0.16	*0.034	0.729	0.075
	AWF	0.31 ± 0.02	0.32 ± 0.02	0.31 ± 0.02	0.053	1.00	0.194
Anterior corona radiata (left)	FA	0.37 ± 0.04	0.39 ± 0.03	0.36 ± 0.02	*0.004	0.989	*<0.001
	RD	0.84 ± 0.13	0.75 ± 0.06	0.84 ± 0.10	*0.003	0.908	*0.049
	RK	1.13 ± 0.10	1.20 ± 0.08	1.08 ± 0.11	*0.007	0.721	*0.008
	AWF	0.31 ± 0.02	0.32 ± 0.02	0.30 ± 0.02	*0.002	0.970	*0.011
Superior corona radiata (right)	FA	0.45 ± 0.03	0.46 ± 0.03	0.48 ± 0.04	0.820	0.093	0.141
	RD	0.65 ± 0.06	0.64 ± 0.10	0.69 ± 0.10	0.915	0.773	0.621
	RK	1.46 ± 0.07	1.46 ± 0.08	1.45 ± 0.13	0.993	0.980	0.991
	AWF	0.38 ± 0.02	0.38 ± 0.02	0.37 ± 0.02	0.887	0.996	0.783
Superior corona radiata (left)	FA	0.45 ± 0.02	0.46 ± 0.03	0.48 ± 0.03	0.484	*0.046	0.218
	RD	0.68 ± 0.07	0.65 ± 0.08	0.71 ± 0.09	0.254	0.796	0.178
	RK	1.42 ± 0.04	1.46 ± 0.09	1.43 ± 0.10	0.187	0.870	0.797
	AWF	0.37 ± 0.01	0.38 ± 0.02	0.37 ± 0.02	0.113	0.942	0.380

This is noted particularly in the fornix and genu of the corpus callosum. Widespread changes were observed in multiple white matter tracts. ANCOVA, covarying for age and sex, corrected for multiple comparisons of combinations of 2 groups using Tukey's HSD. Statistical significance is denoted by *.
Key: AWF, axonal water fraction; CC, corpus callosum; FA, fractional anisotropy; RD, radial diffusivity; RK, radial kurtosis; ROI, region of interest.

clinical status (determined by the GDS) as a covariate, suggesting that they cannot be explained in terms of cognitive impairment but rather are directly related to Aβ burden, which is in agreement with previous studies in either cognitively healthy controls (Racine et al., 2014; Wolf et al., 2015) or mixed cohorts with status being accounted for (Chao et al., 2013; Pietroboni et al., 2017). Because the relationship of WM changes with respect to Aβ burden was not altered by the inclusion of GDS as a covariate, this suggests there may be a mechanistic relationship between amyloid burden and white matter degeneration that may not directly link to or potentially precede cognitive decline.

4.1. Mechanistic insights

Inflammatory processes such as microglial activation and reactive astrocytes have been observed in both aging and AD brains as seen histologically in both mice and human WM (Raj et al., 2017). The observed lower RD, and increased FA, RK, and AWF of global WM tracts, particularly the genu of the corpus callosum and fornix, in the Aβi group, could potentially be explained as a result of these underlying pathological events (Brun and Englund, 1986). In a validation study of diffusion MRI versus histology in cuprizone-fed mice, a similar association between lower RD and increased FA, RK, and AWF was observed in the corpus callosum during the acute inflammatory demyelinating phase characterized by extensive infiltration and proliferation of microglia (Guglielmetti et al., 2016), where these changes were explained because of increased cellularity and membrane barriers resulting in increased restriction and microscopic complexity. Another possible explanation would be that, in the initial demyelination and inflammation stages, iron release results in shortened T_2 for the extra-axonal space, and thus seemingly increased AWF. When the neurodegeneration stage is reached, AWF decreases because the extra-axonal space is relatively expanded due to the loss of myelin and of axons. This is consistent with the myelin model introduced by Bartzokis (2004, 2011), suggesting that myelin breakdown releases iron, which promotes the development of amyloid plaques, which in turn destroys more myelin until the neurodegenerative stage. Multimodal approaches, combining diffusion with myelin estimates from relaxometry, for example Bouhrara et al. (2018), could provide more complete in vivo assessment of microstructural changes in the AD cascade.

The nonmonotonic trend reported here for DKI and WMTI metrics in WM matches trends reported for other AD biomarkers in gray matter. In particular, a cross-sectional study reported cortical thickening in Aβ+/p-tau- groups (Fortea et al., 2014) and in groups with transitional CSF Aβ levels (Fortea et al., 2011), while a longitudinal study showed reduced rates of cortical atrophy in Aβi compared to normal aging from Aβ− (Pegueroles et al., 2017). Furthermore, a biphasic trajectory has been observed for cortical MD, similar to the one observed in the WM in the present study, in a cross-sectional cohort consisting of healthy controls, MCI subjects, and AD subjects (Montal et al., 2018). Interestingly, here we further observed a trend toward larger hippocampal volume in the Aβi group and lower in the Aβ+ group, which could be interpreted as swelling in the Aβi group (due to increased vascular permeability and/or inflammation), and atrophy in the Aβ+ group. In addition to

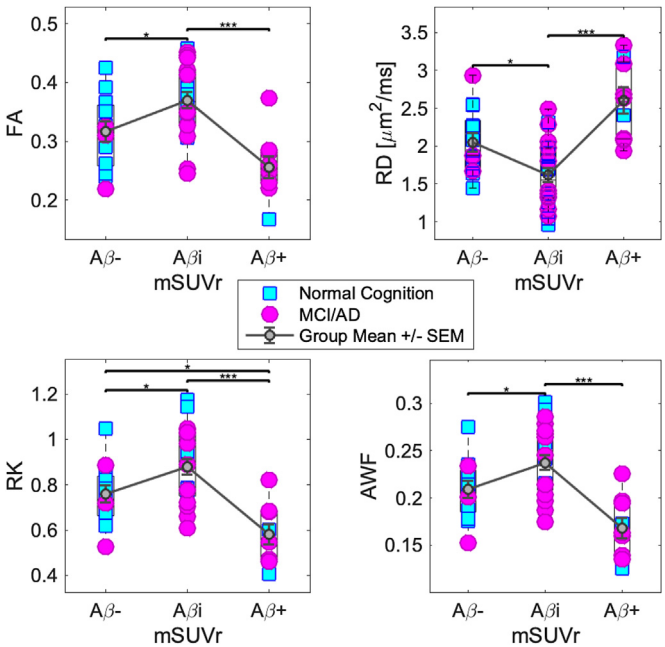

Fig. 3. ROI analysis of the fornix. Observed changes in FA, RD, RK, and AWF are in opposite directions between Aβ−/Aβi and between Aβi/Aβ+ groups. There is lower RD and higher FA, RK, and AWF between the Aβ− and Aβi groups. There is higher RD and lower FA, RK, and AWF between Aβi and Aβ+ groups. Statistical significance is denoted by $^{*}p \leq 0.05$ and $^{***}p \leq 0.001$. Statistics is performed using ANCOVA, covarying for age, with correction for multiple comparison. Group means ± standard errors of the mean are displayed in error bars. Abbreviations: AWF, axonal water fraction; FA, fractional anisotropy; RD, radial diffusivity; ROI, region of interest; RK, radial kurtosis.

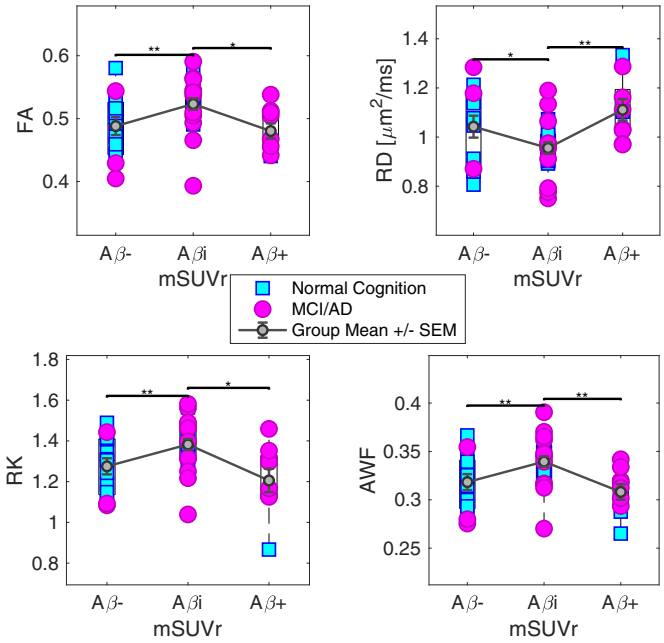

Fig. 4. ROI analysis of the genu of the corpus callosum. Observed changes in FA, RD, RK, and AWF are in opposite directions between Aβ−/Aβi and between Aβi/Aβ+ groups. There is lower RD and higher FA, RK, and AWF between the Aβ− and Aβi groups. There is higher RD and lower FA, RK, and AWF between Aβi and Aβ+ groups. Statistical significance is denoted by $^{*}p \leq 0.01$, and $^{**}p \leq 0.01$. Statistics is performed using ANCOVA, covarying for age, with correction for multiple comparison. Group means ± standard errors of the mean are displayed in error bars. Abbreviations: AWF, axonal water fraction; FA, fractional anisotropy; RD, radial diffusivity; ROI, region of interest; RK, radial kurtosis.

these observations of nonmonotonic (micro)structural changes, cerebral blood flow and hippocampal activation also have been shown to be higher in MCI than in AD and normal aging (Dickerson et al., 2005; Sierra-Marcos, 2017). Although there are no data correlating diffusion with perfusion and fMRI in AD, it is possible that gray matter hyperperfusion and hyperconnectivity in early stages of the disease, which is believed to be part of an initial compensatory mechanism also including pathological elevation of neural activity and release of inflammatory molecules, could parallel the early changes in the white matter that cause an inflammatory response.

Altogether, these findings suggest that the opposing WM diffusion changes that are observed with increasing amyloid burden may be from the fact that inflammation is an early event in AD and that neurodegeneration increases with disease duration and dominates WM diffusion changes later in the disease course. Inflammation may stop or its signature/influence on diffusion MRI parameters may eventually be superseded by the effect of neurodegeneration, including demyelination and axonal loss. Indeed, along with Aβ deposition, AD is also characterized by tau protein misfolding and neurodegenerative processes, including cell death, demyelination, and axonal loss in WM (Brun and Englund, 1986; Englund et al., 1988), which microscopically results in a less restricted and/or hindered space, and thereby higher RD and lower FA, RK, and AWF in the Aβ+ group. Macroscopically, the classical findings of neurodegeneration in AD are cortical and hippocampal atrophy. In agreement, our cohort also showed lower hippocampal volume in the Aβ+ group as compared to the Aβi (and Aβ−) group. Interestingly, in the Aβi as compared to the Aβ− group, we observed a trend toward larger hippocampal volume ($p = 0.06$), and corresponding significant WM differences indicative of higher restriction to diffusion. Similar to findings of biphasic changes in both MD in gray matter and cortical thickness in preclinical AD (Montal et al., 2018), our data support a close relationship between the microstructural WM changes measured with diffusion MRI and macrostructural gray matter changes measured with conventional anatomical MRI. Furthermore, as our results did not change when accounting for cognitive status, these findings point to mechanistic changes that are relatively independent of cognitive status.

4.2. Limitations and future directions

This study may have some limitations that need to be addressed in future research. First, this is a cross-sectional study, and it cannot be assumed that a subject with a certain level of Aβ is temporally similar in clinical manifestation to another subject with the same level of Aβ. Future longitudinal studies combining diffusion MRI with amyloid or tau imaging or CSF markers in individual subjects should better elucidate how WM microstructure changes over time and the underlying pathogenesis. Studying tau would be particularly valuable as this protein has been proposed as the confounding factor explaining the nonlinear trajectory of changes in cortical gray matter (Fortea et al., 2014).

Second, cardiovascular disease may have influenced the diffusion metrics. As cardiovascular diseases are neither static nor binary entities (e.g., diabetes, hypertension, and other cardiovascular diseases range widely in severity, and can fluctuate over time), we chose to quantitatively measure leukoaraiosis (i.e., periventricular and subcortical white matter FLAIR hyperintensity) to characterize cerebral effects from cardiovascular disease burden and found no effect at the group level. APOE4 status is an independent risk factor for cerebral amyloid deposition and has been associated with the

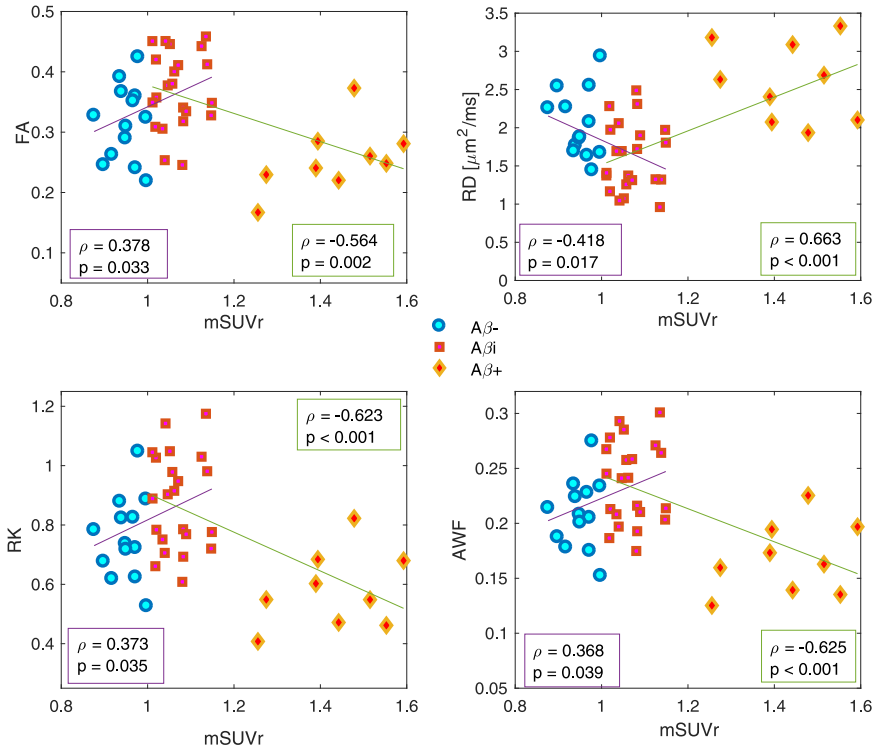

Fig. 5. Correlation analysis of diffusion metrics in the fornix versus mSUVr in combined Aβ− and Aβi groups (cohort 1), and combined Aβi and Aβ+ groups (cohort 2), which demonstrate that correlation coefficients (corrected for age, sex, and Global Deterioration Scale) are significant and in opposite directions for the 2 cohorts. Each plot illustrates the correlation with mSUVr for FA (top left), RD (top right), RK (bottom left), and AWF (bottom right). Abbreviations: AWF, axonal water fraction; FA, fractional anisotropy; RD, radial diffusivity; RK, radial kurtosis.

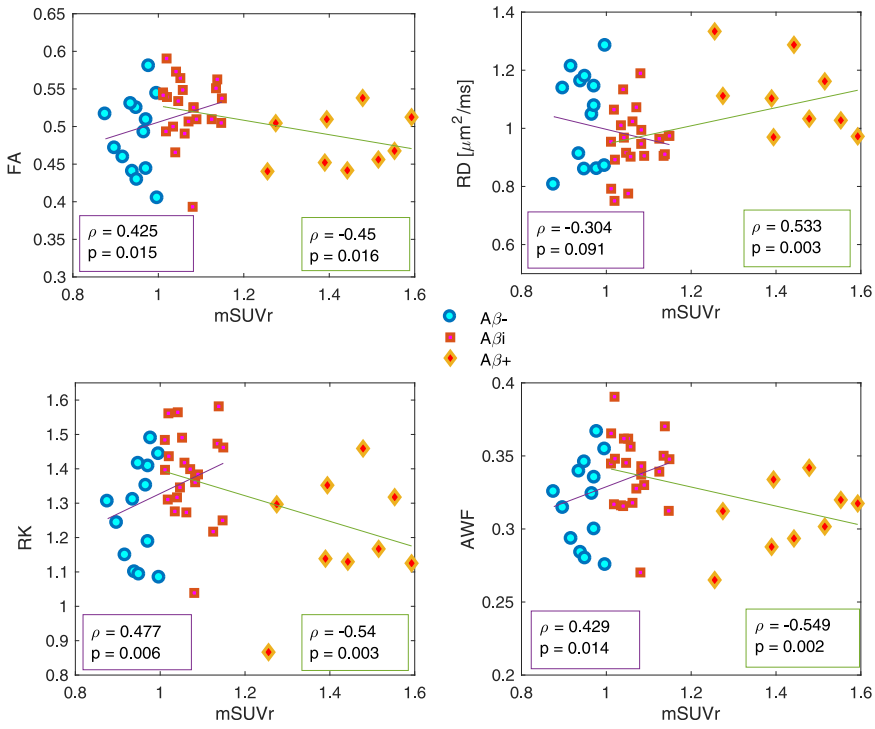

Fig. 6. Correlation analysis of diffusion metrics in the genu versus mSUVr in combined Aβ− and Aβi groups (cohort 1), and combined Aβi and Aβ+ groups (cohort 2), which demonstrate that correlation coefficients (corrected for age, sex, and Global Deterioration Scale) are significant and in opposite directions for the 2 cohorts. Each plot illustrates the correlation with mSUVr for FA (top left), RD (top right), RK (bottom left), and AWF (bottom right). Abbreviations: AWF, axonal water fraction; FA, fractional anisotropy; RD, radial diffusivity; RK, radial kurtosis.

progression of white matter hyperintensities in AD. Unfortunately, no APOE genotype data were available in our cohort.

Third, our limited sample size necessitates to some extent the quantitative categorization of the cerebral amyloid burden, which is a continuous variable by nature, though continuous sampling was not achieved in our sample size (shown in Fig. 1). Although statistically significant changes were observed, the relatively small sample size of our study may limit the generalizability of our results.

Finally, our study includes subjects from 3 different global stages of cognition (as per the GDS scale), which may complicate the interpretation of the relationship between WM integrity and Aβ burden, because subjects with different cognitive status might have different neurodegeneration and neuropathological burden such as tau. Owing to our sample size, limiting the analysis to subjects with the same level of cognition would have resulted in underpowering the study, as discussed in the previous limitation. We emphasize however that our findings were not altered when including GDS as a covariate in the analyses, which means GDS did not have a notable influence over the relationship between WM integrity and amyloid burden.

5. Conclusion

White matter diffusion-derived kurtosis and white matter tract integrity parameters change in opposite directions between Aβ low and Aβ intermediate, and between Aβ intermediate and Aβ high cohorts, respectively, suggesting that different mechanisms affect WM microstructure during different stages of AD. For low Aβ deposition, mechanisms including microglial activation may restrict diffusion, while later on, neurodegenerative effects such as demyelination and axonal loss may dominate and result in less restricted diffusion. The study results emphasize that WM injury occurs in the preclinical or early clinical stages of AD and that diffusion-derived kurtosis and white matter tract integrity parameters may provide useful quantitative biomarkers of early AD.

Disclosure statement

Els Fieremans and Dmitry S. Novikov are coinventors and New York University School of Medicine (NYUSoM) is owner in the denoising technology used in this manuscript as part of the routine data image processing; a patent application has been filed and is pending. Els Fieremans, Timothy M. Shepherd, and Dmitry S. Novikov, and NYUSoM are shareholders and have advisory roles at Microstructure Imaging, Inc. Other authors do not have any potential conflict to disclose.

Acknowledgements

The authors thank Emma Ben-Avi, Sonja Blum, MD, Tracy Butler, MD, Stephanie Chrisphonte, MD, Patrick Harvey, Thet Oo, MBBS, Matthew Lustberg, Martin Sadowski, MD, PhD, Jacqueline Smith, Alok Vedvyas, and Thomas M. Wisniewski, MD, for help with subject recruitment, Kimberly Jackson for technical assistance with data acquisition, and Thomas Vahle for assistance with PET image reconstruction.

The radiotracer Amyvid (florbetapir) was provided to the study by Avid Radiopharmaceuticals Inc, Philadelphia, PA, USA. This work was supported by the Alzheimer Drug Discovery Foundation (EF), NIH NIA K23AG048622 (TMS), NIH NINDS R01NS088040 (EF and DSN), NIH NIA R01AG040211 (JEG), R01AG056531 (EF and RSO), and R01AG056031 (EF and RSO). This work was also supported in part by the Center for Advanced Imaging Innovation and Research, an NIH NIBIB Biomedical Technology Resource Center (P41EB017183), and also benefitted from the Alzheimer's Disease Core Center program grant (P30AG00851).

Authors' contributions: JWD contributed to methodology, formal analysis, writing - original draft, visualization. IOJ contributed to methodology, software, formal analysis, writing - original draft, visualization, investigation. BAA contributed to methodology, software, formal analysis, visualization. DSN contributed to methodology, writing - review & editing. KF contributed to writing - review & editing. JSB contributed to formal analysis. RSO contributed to writing - review & editing. JEG contributed to writing - review & editing, resources. TMS contributed to writing - review & editing. EF contributed to conceptualization, methodology, writing - review & editing, supervision, funding acquisition.

Appendix A. Supplementary data

Supplementary data associated with this article can be found, in the online version, at https://doi.org/10.1016/j.neurobiolaging.2020.01.009.

References

Aasheim, L.B., Karlberg, A., Goa, P.E., Haberg, A., Sorhaug, S., Fagerli, U.M., Eikenes, L., 2015. PET/MR brain imaging: evaluation of clinical UTE-based attenuation correction. Eur. J. Nucl. Med. Mol. Imaging 42, 1439–1446.

Agosta, F., Pievani, M., Sala, S., Geroldi, C., Galluzzi, S., Frisoni, G.B., Filippi, M., 2011. White matter damage in Alzheimer disease and its relationship to gray matter atrophy. Radiology 258, 853–863.

Albert, M.S., DeKosky, S.T., Dickson, D., Dubois, B., Feldman, H.H., Fox, N.C., Gamst, A., Holtzman, D.M., Jagust, W.J., Petersen, R.C., Snyder, P.J., Carrillo, M.C., Thies, B., Phelps, C.H., 2011. The diagnosis of mild cognitive impairment due to Alzheimer's disease: recommendations from the National Institute on Aging-Alzheimer's Association workgroups on diagnostic guidelines for Alzheimer's disease. Alzheimers Dement. 7, 270–279.

Andersson, J.L.R., Jenkinson, M., Smith, S., 2007. Non-linear Registration Aka Spatial Normalisation: FMRIB Technical Report TR07JA2. https://www.fmrib.ox.ac.uk/datasets/techrep/tr07ja2/tr07ja2.pdf. (Accessed 28 June 2007).

Andersson, J.L.R., Sotiropoulos, S.N., 2016. An integrated approach to correction for off-resonance effects and subject movement in diffusion MR imaging. Neuroimage 125, 1063–1078.

Bartzokis, G., 2004. Age-related myelin breakdown: a developmental model of cognitive decline and Alzheimer's disease. Neurobiol. Aging 25, 5–18.

Bartzokis, G., 2011. Alzheimer's disease as homeostatic responses to age-related myelin breakdown. Neurobiol. Aging 32, 1341–1371.

Basser, P.J., Pierpaoli, C., 1996. Microstructural and physiological features of tissues elucidated by quantitative-diffusion-tensor MRI. J. Magn. Reson. B 111, 209–219.

Benitez, A., Fieremans, E., Jensen, J.H., Falangola, M.F., Tabesh, A., Ferris, S.H., Helpern, J.A., 2013. White matter tract integrity metrics reflect the vulnerability of late-myelinating tracts in Alzheimer's disease. Neuroimage. Clin. 4, 64–71.

Benitez, A., Jensen, J.H., Falangola, M.F., Nietert, P.J., Helpern, J.A., 2018. Modeling white matter tract integrity in aging with diffusional kurtosis imaging. Neurobiol. Aging 70, 265–275.

Bilello, M., Doshi, J., Nabavizadeh, S.A., Toledo, J.B., Erus, G., Xie, S.X., Trojanowski, J.Q., Han, X., Davatzikos, C., 2015. Correlating cognitive decline with white matter lesion and brain atrophy magnetic resonance imaging measurements in alzheimer's disease. J. Alzheimers Dis. 48, 987–994.

Bilgel, M., An, Y., Helphrey, J., Elkins, W., Gomez, G., Wong, D.F., Davatzikos, C., Ferrucci, L., Resnick, S.M., 2018. Effects of amyloid pathology and neurodegeneration on cognitive change in cognitively normal adults. Brain. 141, 2475–2485.

Bouhrara, M., Reiter, D.A., Bergeron, C.M., Zukley, L.M., Ferrucci, L., Resnick, S.M., Spencer, R.G., 2018. Evidence of demyelination in mild cognitive impairment and dementia using a direct and specific magnetic resonance imaging measure of myelin content. Alzheimers Dement. 14, 998–1004.

Brun, A., Englund, E., 1986. A white matter disorder in dementia of the Alzheimer type: a pathoanatomical study. Ann. Neurol. 19, 253–262.

Chang, Y.L., Chen, T.F., Shih, Y.C., Chiu, M.J., Yan, S.H., Tseng, W.Y., 2015. Regional cingulum disruption, not gray matter atrophy, detects cognitive changes in amnestic mild cognitive impairment subtypes. J. Alzheimers Dis. 44, 125–138.

Chao, L.L., DeCarli, C., Kriger, S., Truran, D., Zhang, Y., Laxamana, J., Villeneuve, S., Jagust, W.J., Sanossian, N., Mack, W.J., Chui, H.C., Weiner, M.W., 2013. Associations between white matter hyperintensities and β amyloid on integrity of projection, association, and limbic fiber tracts measured with diffusion tensor MRI. PLoS One 8, e65175.

Clark, C.M., Pontecorvo, M.J., Beach, T.G., Bedell, B.J., Coleman, R.E., Doraiswamy, P.M., Fleisher, A.S., Reiman, E.M., Sabbagh, M.N., Sadowsky, C.H., Schneider, J.A., Arora, A., Carpenter, A.P., Flitter, M.L., Joshi, A.D., Krautkramer, M.J., Lu, M., Mintun, M.A., Skovronsky, D.M., 2012. Cerebral PET with florbetapir compared with neuropathology at autopsy for detection of neuritic amyloid-β plaques: a prospective cohort study. Lancet Neurol. 11, 669–678.

Clark, C.M., Schneider, J.A., Bedell, B.J., Beach, T.G., Bilker, W.B., Mintun, M.A., Pontecorvo, M.J., Hefti, F., Carpenter, A.P., Flitter, M.L., Krautkramer, M.J., Kung, H.F., Coleman, R.E., Doraiswamy, P.M., Fleisher, A.S., Sabbagh, M.N., Sadowsky, C.H., Reiman, E.P., Reiman, P.E.M., Zehntner, S.P., Skovronsky, D.M., AV45-A07 Study Group, 2011. Use of florbetapir-PET for imaging beta-amyloid pathology. JAMA 305, 275–283.

Curtis, C., Gamez, J.E., Singh, U., Sadowsky, C.H., Villena, T., Sabbagh, M.N., Beach, T.G., Duara, R., Fleisher, A.S., Frey, K.A., Walker, Z., Hunjan, A., Holmes, C., Escovar, Y.M., Vera, C.X., Agronin, M.E., Ross, J., Bozoki, A., Akinola, M., Shi, J., Vandenberghe, R., Ikonomovic, M.D., Sherwin, P.F., Grachev, I.D., Farrar, G., Smith, A.P.L., Buckley, C.J., McLain, R., Salloway, S., 2015. Phase 3 trial of flutemetamol labeled with radioactive fluorine 18 imaging and neuritic plaque density. JAMA Neurol. 72, 287–294.

Di Paola, M., Phillips, O., Orfei, M.D., Piras, F., Cacciari, C., Caltagirone, C., Spalletta, G., 2015. Corpus callosum structure is topographically correlated with the early course of cognition and depression in alzheimer's disease. J. Alzheimers Dis. 45, 1097–1108.

Dickerson, B.C., Salat, D.H., Greve, D.N., Chua, E.F., Rand-Giovannetti, E., Rentz, D.M., Bertram, L., Mullin, K., Tanzi, R.E., Blacker, D., Albert, M.S., Sperling, R.A., 2005. Increased hippocampal activation in mild cognitive impairment compared to normal aging and AD. Neurology 65, 404.

Englund, E., Brun, A., Alling, C., 1988. White matter changes in dementia of Alzheimer's type. Biochemical and neuropathological correlates. Brain 111 (Pt 6), 1425–1439.

Fieremans, E., Jensen, J.H., Helpern, J.A., 2011. White matter characterization with diffusional kurtosis imaging. Neuroimage 58, 177–188.

Fieremans, E., Benitez, A., Jensen, J.H., Falangola, M.F., Tabesh, A., Deardorff, R.L., Spampinato, M.V., Babb, J.S., Novikov, D.S., Ferris, S.H., Helpern, J.A., 2013. Novel white matter tract integrity metrics sensitive to Alzheimer disease progression. AJNR. Am. J. Neuroradiol. 34, 2105–2112.

Fleisher, A.S., Chen, K., Liu, X., Roontiva, A., Thiyyagura, P., Ayutyanont, N., Joshi, A.D., Clark, C.M., Mintun, M.A., Pontecorvo, M.J., Doraiswamy, P.M., Johnson, K.A., Skovronsky, D.M., Reiman, E.M., 2011. Using positron emission tomography and florbetapir f 18 to image cortical amyloid in patients with mild cognitive impairment or dementia due to alzheimer disease. Arch. Neurol. 68, 1404–1411.

Fortea, J., Sala-Llonch, R., Bartrés-Faz, D., Lladó, A., Solé-Padullés, C., Bosch, B., Antonell, A., Olives, J., Sanchez-Valle, R., Molinuevo, J.L., Rami, L., 2011. Cognitively preserved subjects with transitional cerebrospinal fluid ß-amyloid 1-42 values have thicker cortex in alzheimer's disease vulnerable areas. Biol. Psychiatry 70, 183–190.

Fortea, J., Vilaplana, E., Alcolea, D., Carmona-Iragui, M., Sánchez-Saudinos, M.-B., Sala, I., Antón-Aguirre, S., González, S., Medrano, S., Pegueroles, J., Morenas, E., Clarimón, J., Blesa, R., Lleó, A., Alzheimer's Disease Neuroimaging Initiative, 2014. Cerebrospinal fluid β-amyloid and phospho-tau biomarker interactions affecting brain structure in preclinical Alzheimer disease. Ann. Neurol. 76, 223–230.

Gottfries, C.G., Karlsson, I., Svennerholm, L., 1996. Membrane components separate early-onset Alzheimer's disease from senile dementia of the Alzheimer type. Int. Psychogeriatr. 8, 365–372.

Guglielmetti, C., Veraart, J., Roelant, E., Mai, Z., Daans, J., Van Audekerke, J., Naeyaert, M., Vanhoutte, G., Delgado y Palacios, R., Praet, J., Fieremans, E., Ponsaerts, P., Sijbers, J., Van der Linden, A., Verhoye, M., 2016. Diffusion kurtosis imaging probes cortical alterations and white matter pathology following cuprizone induced demyelination and spontaneous remyelination. Neuroimage 125, 363–377.

Jack, C.R., Knopman, D.S., Jagust, W.J., Petersen, R.C., Weiner, M.W., Aisen, P.S., Shaw, L.M., Vemuri, P., Wiste, H.J., Weigand, S.D., Lesnick, T.G., Pankratz, V.S., Donohue, M.C., Trojanowski, J.Q., 2013. Tracking pathophysiological processes in Alzheimer's disease: an updated hypothetical model of dynamic biomarkers. Lancet Neurol. 12, 207–216.

Jack, C.R., Bennett, D.A., Blennow, K., Carrillo, M.C., Dunn, B., Haeberlein, S.B., Holtzman, D.M., Jagust, W., Jessen, F., Karlawish, J., Liu, E., Molinuevo, J.L., Montine, T., Phelps, C., Rankin, K.P., Rowe, C.C., Scheltens, P., Siemers, E., Snyder, H.M., Sperling, R., 2018. NIA-AA Research Framework: toward a biological definition of Alzheimer's disease. Alzheimers Dement. 14, 535–562.

Jelescu, I.O., Veraart, J., Adisetiyo, V., Milla, S.S., Novikov, D.S., Fieremans, E., 2015. One diffusion acquisition and different white matter models: how does microstructure change in human early development based on WMTI and NODDI? Neuroimage 107, 242–256.

Jelescu, I.O., Veraart, J., Fieremans, E., Novikov, D.S., 2016a. Degeneracy in model parameter estimation for multi-compartmental diffusion in neuronal tissue. NMR Biomed. 29, 33–47.

Jelescu, I.O., Zurek, M., Winters, K.V., Veraart, J., Rajaratnam, A., Kim, N.S., Babb, J.S., Shepherd, T.M., Novikov, D.S., Kim, S.G., Fieremans, E., 2016b. In vivo quantification of demyelination and recovery using compartment-specific diffusion MRI metrics validated by electron microscopy. Neuroimage 132, 104–114.

Jenkinson, M., Bannister, P., Brady, M., Smith, S., 2002. Improved optimization for the robust and accurate linear registration and motion correction of brain images. Neuroimage 17, 825–841.

Jenkinson, M., Beckmann, C.F., Behrens, T.E., Woolrich, M.W., Smith, S.M., 2012. FSL. Neuroimage 62, 782–790.

Jensen, J.H., Helpern, J.A., 2010. MRI quantification of non-Gaussian water diffusion by kurtosis analysis. NMR Biomed. 23, 698–710.

Joshi, A.D., Pontecorvo, M.J., Clark, C.M., Carpenter, A.P., Jennings, D.L., Sadowsky, C.H., Adler, L.P., Kovnat, K.D., Seibyl, J.P., Arora, A., Saha, K., Burns, J.D., Lowrey, M.J., Mintun, M.A., Skovronsky, D.M., 2012. Performance characteristics of amyloid PET with florbetapir F 18 in patients with alzheimer's disease and cognitively normal subjects. J. Nucl. Med. 53, 378–384.

Kantarci, K., Schwarz, C.G., Reid, R.I., Przybelski, S.A., Lesnick, T.G., Zuk, S.M., Senjem, M.L., Gunter, J.L., Lowe, V., Machulda, M.M., Knopman, D.S., Petersen, R.C., Jack, C.R., 2014. White matter integrity determined with diffusion tensor imaging in older adults without dementia: influence of amyloid load and neurodegeneration. JAMA Neurol. 71, 1547–1554.

Kellner, E., Dhital, B., Kiselev, V.G., Reisert, M., 2016. Gibbs-ringing artifact removal based on local subvoxel-shifts. Magn. Reson. Med. 76, 1574–1581.

Kemper, T.L., 1994. Neuroanatomical and Neuropathological Changes during Aging and Dementia, Clinical Neurology of Aging, second ed. Oxford University Press, New York, NY, pp. 3–67.

Kobayashi, K., Hayashi, M., Nakano, H., Fukutani, Y., Sasaki, K., Shimazaki, M., Koshino, Y., 2002. Apoptosis of astrocytes with enhanced lysosomal activity and oligodendrocytes in white matter lesions in Alzheimer's disease. Neuropathol. Appl. Neurobiol. 28, 238–251.

Kunz, N., da Silva, A.R., Jelescu, I.O., 2018. Intra- and extra-axonal axial diffusivities in the white matter: which one is faster? Neuroimage 181, 314–322.

Madden, D.J., Bennett, I.J., Song, A.W., 2009. Cerebral white matter integrity and cognitive aging: contributions from diffusion tensor imaging. Neuropsychol. Rev. 19, 415.

Malone, M.J., Szoke, M.C., 1985. Neurochemical changes in white matter. Aged human brain and Alzheimer's disease. Arch. Neurol. 42, 1063–1066.

Mayo, C.D., Mazerolle, E.L., Ritchie, L., Fisk, J.D., Gawryluk, J.R., 2017. Longitudinal changes in microstructural white matter metrics in Alzheimer's disease. Neuroimage Clin. 13, 330–338.

McKhann, G.M., Knopman, D.S., Chertkow, H., Hyman, B.T., Jack Jr., C.R., Kawas, C.H., Klunk, W.E., Koroshetz, W.J., Manly, J.J., Mayeux, R., Mohs, R.C., Morris, J.C., Rossor, M.N., Scheltens, P., Carrillo, M.C., Thies, B., Weintraub, S., Phelps, C.H., 2011. The diagnosis of dementia due to Alzheimer's disease: recommendations from the National Institute on Aging-Alzheimer's Association workgroups on diagnostic guidelines for Alzheimer's disease. Alzheimers Dement. 7, 263–269.

McKinnon, E.T., Helpern, J.A., Jensen, J.H., 2018. Modeling white matter microstructure with fiber ball imaging. Neuroimage 176, 11–21.

Mielke, M.M., Kozauer, N.A., Chan, K.C., George, M., Toroney, J., Zerrate, M., Bandeen-Roche, K., Wang, M.C., Vanzijl, P., Pekar, J.J., Mori, S., Lyketsos, C.G., Albert, M., 2009. Regionally-specific diffusion tensor imaging in mild cognitive impairment and Alzheimer's disease. Neuroimage 46, 47–55.

Mielke, M.M., Okonkwo, O.C., Oishi, K., Mori, S., Tighe, S., Miller, M.I., Ceritoglu, C., Brown, T., Albert, M., Lyketsos, C.G., 2012. Fornix integrity and hippocampal volume predict memory decline and progression to Alzheimer's disease. Alzheimers Dement. 8, 105–113.

Mikheev, A., Nevsky, G., Govindan, S., Grossman, R., Rusinek, H., 2008. Fully automatic segmentation of the brain from T1-weighted MRI using Bridge Burner Algorithm. J. Magn. Reson. Imaging 27, 1235–1241.

Mito, R., Raffelt, D., Dhollander, T., Vaughan, D.N., Tournier, J.D., Salvado, O., Brodtmann, A., Rowe, C.C., Villemagne, V.L., Connelly, A., 2018. Fibre-specific white matter reductions in Alzheimer's disease and mild cognitive impairment. Brain 141, 888–902.

Montal, V., Vilaplana, E., Alcolea, D., Pegueroles, J., Pasternak, O., Gonzalez-Ortiz, S., Clarimon, J., Carmona-Iragui, M., Illan-Gala, I., Morenas-Rodriguez, E., Ribosa-Nogue, R., Sala, I., Sanchez-Saudinos, M.B., Garcia-Sebastian, M., Villanua, J., Izagirre, A., Estanga, A., Ecay-Torres, M., Iriondo, A., Clerigue, M., Tainta, M., Pozueta, A., Gonzalez, A., Martinez-Heras, E., Llufriu, S., Blesa, R., Sanchez-Juan, P., Martinez-Lage, P., Lleo, A., Fortea, J., 2018. Cortical microstructural changes along the Alzheimer's disease continuum. Alzheimers Dement. 14, 340–351.

Mori, S., Oishi, K., Jiang, H., Jiang, L., Li, X., Akhter, K., Hua, K., Faria, A.V., Mahmood, A., Woods, R., Toga, A.W., Pike, G.B., Neto, P.R., Evans, A., Zhang, J., Huang, H., Miller, M.I., van Zijl, P., Mazziotta, J., 2008. Stereotaxic white matter atlas based on diffusion tensor imaging in an ICBM template. Neuroimage 40, 570–582.

Morris, J.C., Weintraub, S., Chui, H.C., Cummings, J., Decarli, C., Ferris, S., Foster, N.L., Galasko, D., Graff-Radford, N., Peskind, E.R., Beekly, D., Ramos, E.M., Kukull, W.A., 2006. The Uniform data Set (UDS): clinical and cognitive variables and descriptive data from alzheimer disease centers. Alzheimer Dis. Assoc. Disord. 20, 210–216.

Novikov, D.S., Veraart, J., Jelescu, I.O., Fieremans, E., 2018. Rotationally-invariant mapping of scalar and orientational metrics of neuronal microstructure with diffusion MRI. Neuroimage 174, 518–538.

Novikov, D.S., Fieremans, E., Jespersen, S.N., Kiselev, V.G., 2019. Quantifying brain microstructure with diffusion MRI: theory and parameter estimation. NMR Biomed. 32, e3998.

Oishi, K., Lyketsos, C.G., 2014. Alzheimer's disease and the fornix. Front Aging Neurosci. 6, 241.

Pegueroles, J., Vilaplana, E., Montal, V., Sampedro, F., Alcolea, D., Carmona-Iragui, M., Clarimon, J., Blesa, R., Lleo, A., Fortea, J., 2017. Longitudinal brain structural changes in preclinical Alzheimer's disease. Alzheimers Dement. 13, 499–509.

Petersen, R.C., Doody, R., Kurz, A., Mohs, R.C., Morris, J.C., Rabins, P.V., Ritchie, K., Rossor, M., Thal, L., Winblad, B., 2001. Current concepts in mild cognitive impairment. Arch. Neurol. 58, 1985–1992.

Pietroboni, A.M., Scarioni, M., Carandini, T., Basilico, P., Cadioli, M., Giulietti, G., Arighi, A., Caprioli, M., Serra, L., Sina, C., Fenoglio, C., Ghezzi, L., Fumagalli, G.G.,

De Riz, M.A., Calvi, A., Triulzi, F., Bozzali, M., Scarpini, E., Galimberti, D., 2017. CSF β-amyloid and white matter damage: a new perspective on Alzheimer's disease. J. Neurol. Neurosurg. Psychiatry 89, 352–357.
Racine, A.M., Adluru, N., Alexander, A.L., Christian, B.T., Okonkwo, O.C., Oh, J., Cleary, C.A., Birdsill, A., Hillmer, A.T., Murali, D., Barnhart, T.E., Gallagher, C.L., Carlsson, C.M., Rowley, H.A., Dowling, N.M., Asthana, S., Sager, M.A., Bendlin, B.B., Johnson, S.C., 2014. Associations between white matter microstructure and amyloid burden in preclinical Alzheimer's disease: a multimodal imaging investigation. Neuroimage. Clin. 4, 604–614.
Raj, D., Yin, Z., Breur, M., Doorduin, J., Holtman, I.R., Olah, M., Mantingh-Otter, I.J., Van Dam, D., De Deyn, P.P., den Dunnen, W., Eggen, B.J.L., Amor, S., Boddeke, E., 2017. Increased white matter inflammation in aging- and Alzheimer's disease brain. Front Mol. Neurosci. 10, 206.
Reisberg, B., Ferris, S.H., de Leon, M.J., Crook, T., 1982. The Global Deterioration Scale for assessment of primary degenerative dementia. Am. J. Psychiatry 139, 1136–1139.
Roher, A.E., Weiss, N., Kokjohn, T.A., Kuo, Y.M., Kalback, W., Anthony, J., Watson, D., Luehrs, D.C., Sue, L., Walker, D., Emmerling, M., Goux, W., Beach, T., 2002. Increased A beta peptides and reduced cholesterol and myelin proteins characterize white matter degeneration in Alzheimer's disease. Biochemistry 41, 11080–11090.
Sabri, O., Seibyl, J., Rowe, C., Barthel, H., 2015. Beta-amyloid imaging with florbetaben. Clin. Transl. Imaging 3, 13–26.
Sierra-Marcos, A., 2017. Regional cerebral blood flow in mild cognitive impairment and alzheimer's disease measured with arterial spin labeling magnetic resonance imaging. Int. J. Alzheimers Dis. 2017, 5479597.
Smith, S.M., Jenkinson, M., Johansen-Berg, H., Rueckert, D., Nichols, T.E., Mackay, C.E., Watkins, K.E., Ciccarelli, O., Cader, M.Z., Matthews, P.M., Behrens, T.E.J., 2006. Tract-based spatial statistics: Voxelwise analysis of multi-subject diffusion data. Neuroimage 31, 1487–1505.
Smith, S.M., Nichols, T.E., 2009. Threshold-free cluster enhancement: addressing problems of smoothing, threshold dependence and localisation in cluster inference. Neuroimage 44, 83–98.
Sperling, R.A., Aisen, P.S., Beckett, L.A., Bennett, D.A., Craft, S., Fagan, A.M., Iwatsubo, T., Jack Jr., C.R., Kaye, J., Montine, T.J., Park, D.C., Reiman, E.M., Rowe, C.C., Siemers, E., Stern, Y., Yaffe, K., Carrillo, M.C., Thies, B., Morrison-Bogorad, M., Wagster, M.V., Phelps, C.H., 2011. Toward defining the preclinical stages of Alzheimer's disease: recommendations from the National Institute on Aging-Alzheimer's Association workgroups on diagnostic guidelines for Alzheimer's disease. Alzheimers Dement. 7, 280–292.
Svennerholm, L., Gottfries, C.G., 1994. Membrane lipids, selectively diminished in Alzheimer brains, suggest synapse loss as a primary event in early-onset form (type I) and demyelination in late-onset form (type II). J. Neurochem. 62, 1039–1047.
Veraart, J., Sijbers, J., Sunaert, S., Leemans, A., Jeurissen, B., 2013. Weighted linear least squares estimation of diffusion MRI parameters: strengths, limitations, and pitfalls. Neuroimage 81, 335–346.
Veraart, J., Fieremans, E., Novikov, D.S., 2016a. Diffusion MRI noise mapping using random matrix theory. Magn. Reson. Med. 76, 1582–1593.
Veraart, J., Novikov, D.S., Christiaens, D., Ades-aron, B., Sijbers, J., Fieremans, E., 2016b. Denoising of diffusion MRI using random matrix theory. Neuroimage 142, 394–406.
Weintraub, S., Salmon, D., Mercaldo, N., Ferris, S., Graff-Radford, N.R., Chui, H., Cummings, J., DeCarli, C., Foster, N.L., Galasko, D., Peskind, E., Dietrich, W., Beekly, D.L., Kukull, W.A., Morris, J.C., 2009. The alzheimer's disease centers' Uniform data Set (UDS): the neuropsychologic test battery. Alzheimer Dis. Assoc. Disord. 23, 91–101.
Winkler, A.M., Ridgway, G.R., Webster, M.A., Smith, S.M., Nichols, T.E., 2014. Permutation inference for the general linear model. Neuroimage 92, 381–397.
Wolf, D., Fischer, F.U., Scheurich, A., Fellgiebel, A., 2015. Non-linear association between cerebral amyloid deposition and white matter microstructure in cognitively healthy older adults. J. Alzheimers Dis. 47, 117–127.
Wong, D.F., Rosenberg, P.B., Zhou, Y., Kumar, A., Raymont, V., Ravert, H.T., Dannals, R.F., Nandi, A., Brasic, J.R., Ye, W., Hilton, J., Lyketsos, C., Kung, H.F., Joshi, A.D., Skovronsky, D.M., Pontecorvo, M.J., 2010. In vivo imaging of amyloid deposition in Alzheimer disease using the radioligand 18F-AV-45 (florbetapir [corrected] F 18). J. Nucl. Med. 51, 913–920.
Wurtman, R., 2015. Biomarkers in the diagnosis and management of Alzheimer's disease. Metab. Clin. Exp. 64 (3 Suppl 1), S47–S50.